Importance of the spin-orbit split-off band on the tunneling properties of holes through $Al_xGa_{1-x}As/GaAs$ and $InP/In_yGa_{1-y}As$ heterostructures

S. Ekbote, M. Cahay, and K. Roenker
Department of Electrical Engineering, University of Cincinnati, Cincinnati, Ohio 45221
(Received 3 November 1997; revised manuscript received 10 August 1998)

The influence of the spin-orbit split-off band on the tunneling of holes across heterostructures is studied starting with the 6×6 Luttinger-Kohn Hamiltonian. The latter is diagonalized into 3×3 blocks (upper and lower Hamiltonians) using a unitary transformation. We consider $Al_xGa_{1-x}As/GaAs$ and $InP/In_yGa_{1-y}As$ material systems, and study the tunneling of holes through a one-dimensional δ scatterer and across abrupt potential steps. In each case, we show that the presence of the spin-orbit split-off band has a profound influence on the transmission coefficients of holes, even for holes with energy much lower than the threshold for free propagation in the spin-orbit split-off band. For the potential steps, we show that the results can be quite different with upper and lower Hamiltonians. Furthermore, we stress the importance of the spin-orbit split-off band by comparing the results with those obtained with the 4×4 Luttinger-Kohn Hamiltonian which neglects the importance of the spin-orbit split-off band.
[S0163-1829(98)08148-X]

I. INTRODUCTION

In the past, there have been only a few reports on the treatment of hole tunneling in realistic structures based on the transfer-matrix formalism following the original $\mathbf{k}\cdot\mathbf{p}$ model.[1] Starting with the 4×4 Luttinger-Kohn Hamiltonian, Chuang used a transfer-matrix approach to study the problem of hole tunneling through simple potential steps.[2] He showed that there is a high probability for a hole to change character (heavy to light or the reverse) while tunneling from low-band-gap to higher-band-gap material at a heterojunction interface. On the other hand, the probability of conversion from heavy to light or the reverse is much less for holes incident on an interface from the higher-band-gap material. The transfer-matrix formalism has also been applied to the problem of hole tunneling through resonant tunneling structures.[3–7] These simulations have shown that the transfer-matrix method is numerically unstable for device structures larger than a few tens of Å. To circumvent the difficulties encountered in the transfer-matrix technique, Liu, Ting, and McGill recently proposed the use of the multiband quantum transmitting boundary method (MQTBM).[8] This technique is easy to implement and numerically stable. So far, Liu, Ting, and McGill applied their MQTBM technique only to hole transport through resonant tunneling devices starting with the 4×4 Luttinger-Kohn Hamiltonian. A scattering-matrix to describe hole transport was used recently by Sanchez and Proetto[9] to study hole tunneling through simple barriers and above quantum wells. Recently, we generalized that approach to study hole tunneling across the emitter-base junction of abrupt and graded heterojunction bipolar transistors starting with the 4×4 Luttinger-Kohn Hamiltonian in which only the mixing between heavy and light holes is taken into account.[10]

Chao and Chuang[4] showed that the spin-orbit split-off band has a significant effect on the band structure of quantum wells especially for highly strained quantum wells. Chang and Chuang also showed that the inclusion of the spin-orbit split-off band influences all optoelectronic properties of strained quantum-well lasers (threshold current, gain and absorption spectra).[11] This is mainly a consequence of the substantial change in the energy dispersion relations of holes (even for low values of the hole energy) when the effects of spin-orbit coupling are taken into account. The spin-orbit split-off band should therefore also have an important influence on the transport of holes across a heterostructure even if the hole energy is far below the maximum of the spin-orbit split-off (SO) band.

In this paper, we analyze the effects of the SO band on the tunneling properties of holes through unstrained heterostructures. Recently, Sanchez and Proetto performed an analysis of hole refraction from strained $Si_{1-x}Ge_x/Si$ heterojunctions starting with the 6×6 Luttinger-Kohn Hamiltonian.[12] We perform a similar analysis of $Al_xGa_{1-x}As/GaAs$ and $InP/In_yGa_{1-y}As$ interfaces, which are two of the most widely used material systems in the investigation of ultrafast submicron devices for millimeter wave applications. Our analysis is more complete than the one reported by Sanchez and Proetto because we compare the results obtained with the 6×6 and 4×4 Luttinger-Kohn Hamiltonians, illustrating the dramatic influence of the SO band on the tunneling properties of holes even for carriers with a low kinetic energy. Furthermore, we show that the results obtained with the upper and lower Hamiltonians obtained after performing a unitary transform of the Luttinger-Kohn Hamiltonian are quite different when the heterostructure lacks inversion symmetry.

This paper is organized as follows. In Sec. II, we develop the formalism to calculate the eigenvalues and eigenstates of the 6×6 Luttinger-Kohn Hamiltonian in the axial approximation. In Sec. III, we consider the following problems: (1) hole tunneling through a δ scatterer, and (2) hole tunneling across a potential step. We stress the importance of the spin-orbit split-off band by performing simultaneously the calculations while neglecting it. Finally, Sec. IV contains our conclusions.

II. APPROACH

Following Chao and Chuang,[4] we start with the Luttinger-Kohn Hamiltonian describing the top of the valence band while including the effects of the spin-orbit split-off band

$$H=\begin{bmatrix} P+Q & -S & R & 0 & -\frac{1}{\sqrt{2}}S & \sqrt{2}R \\ -S^{\dagger} & P-Q & 0 & R & -\sqrt{2}Q & \sqrt{\frac{3}{2}}S \\ R^{\dagger} & 0 & P-Q & S & \sqrt{\frac{3}{2}}S^{\dagger} & \sqrt{2}Q \\ 0 & R^{\dagger} & S^{\dagger} & P+Q & -\sqrt{2}R^{\dagger} & -\frac{1}{\sqrt{2}}S^{\dagger} \\ -\frac{1}{\sqrt{2}}S^{\dagger} & -\sqrt{2}Q & \sqrt{\frac{3}{2}}S & -\sqrt{2}R & P+\Delta & 0 \\ \sqrt{2}R^{\dagger} & \sqrt{\frac{3}{2}}S^{\dagger} & \sqrt{2}Q & -\frac{1}{\sqrt{2}}S & 0 & P+\Delta \end{bmatrix} \tag{1}$$

where

$$P=\Gamma_1(k_x^2+k_y^2+k_z^2), \tag{2}$$

$$Q=\Gamma_2(k_x^2+k_y^2-2k_z^2), \tag{3}$$

$$R=-\sqrt{3}\tilde{\Gamma}(k_x-ik_y)^2+\sqrt{3}\left[\frac{\Gamma_3-\Gamma_2}{2}\right](k_x+ik_y)^2 \tag{4}$$

and

$$S=2\sqrt{3}\Gamma_3(k_x-ik_y)k_z, \tag{5}$$

where the wave vector $\mathbf{k}=(k_x,k_y,k_z)$ is interpreted as a differential operator $-i\nabla$. In Eq. (1), Δ is the spin-orbit split-off energy. Furthermore, the following notations were used: $\Gamma_1=\hbar^2\gamma_1/2m$, $\Gamma_2=\hbar^2\gamma_2/2m$, $\Gamma_3=\hbar^2\gamma_3/2m$, and $\tilde{\Gamma}=(\Gamma_2+\Gamma_3)/2$, where γ_i are the Luttinger parameters. Hereafter, hole energies are measured as positive moving into the valence band and taking the top of the valence band as the zero of energy.

The Hamiltonian in Eq. (1) is a 6×6 matrix in the basis composed of $(|\frac{3}{2},\pm\frac{3}{2}\rangle)$ heavy-hole, $(|\frac{3}{2},\pm\frac{1}{2}\rangle)$ light-hole, and $(|\frac{1}{2},\pm\frac{1}{2}\rangle)$ split-off Bloch wave functions at the center of the Brillouin zone. In the axial approximation, the matrix element R in Eq. (1) is approximated by

$$R=-\sqrt{3}\tilde{\Gamma}k_\rho^2\exp(-2i\phi) \tag{6}$$

where $k_\rho^2=k_x^2+k_y^2$ and $\phi=a\tan(k_y/k_x)$. Hamiltonian (1) can be block diagonalized using a similarity transformation as described in Refs. 4 and 5. In the new basis set,[4] the transformed Hamiltonian can then be written as

$$H=\begin{bmatrix} H_{3\times3} & 0 \\ 0 & H_{3\times3}^{\dagger} \end{bmatrix}, \tag{7}$$

where $H_{3\times3}^{\dagger}$ is the Hermitian conjugate of $H_{3\times3}$. The explicit form of the Hamiltonian $H_{3\times3}$ is given by

$$H_{3\times3}=\begin{bmatrix} P+Q & -R_\rho-iS_\rho & -\sqrt{2}R_\rho+\frac{i}{\sqrt{2}}S_\rho \\ -R_\rho+iS_\rho & P-Q & \sqrt{2}Q+i\sqrt{3/2}S_\rho \\ -\sqrt{2}R_\rho-\frac{i}{\sqrt{2}}S_\rho & \sqrt{2}Q-i\sqrt{3/2}S_\rho & P+\Delta \end{bmatrix} \tag{8}$$

where

$$R_\rho=-\sqrt{3}\tilde{\Gamma}k_\rho^2, \tag{9}$$

and

$$S_\rho=2\sqrt{3}\Gamma_3k_\rho k_z. \tag{10}$$

Starting with the upper or lower Hamiltonian, the eigenenergies and corresponding envelope functions of the valence subbands can be obtained by solving the effective-mass equation

$$\Sigma_j[H_{ij}+V_h(z)\delta_{ij}]F_j(\mathbf{k_p},\mathbf{r})=E(k_\rho)F_i(\mathbf{k_p},\mathbf{r}), \tag{11}$$

where $(i,j)=(1,2,3)$, and $V_h(z)$ is the valence-band potential-energy profile. In the axial approximation, the envelope-function components F_j can be approximated as follows:

$$F_j(\mathbf{k}_\rho,\mathbf{r})=F_j(\mathbf{k}_\rho,z)e^{i\mathbf{k}_\rho\cdot\boldsymbol{\rho}}, \tag{12}$$

where z is the direction of growth of the heterostructure. In Eq. (12), $\mathbf{k}_\rho=k_x\mathbf{x}+k_y\mathbf{y}$ and $\boldsymbol{\rho}=x\mathbf{x}+y\mathbf{y}$.

For a fixed energy E and in-plane wave vector $\mathbf{k}_\rho$, Eq. (11) will have three complex wave vector solutions k_z and associated wave vectors $\mathbf{F}(\mathbf{k}_\rho,z)$. We seek solutions of Eq. (11) of the form

$$\mathbf{F}(\mathbf{k}_\rho,z)=\mathbf{F}_\mathbf{k}e^{ik_z z}. \tag{13}$$

Substituting Eq. (13) into Eq. (11), we find that the eigenvectors $\mathbf{F}_k$ must satisfy the eigenvalue problem

$$H_{3\times3}\mathbf{F}_\mathbf{k}=E\mathbf{F}_\mathbf{k}, \tag{14}$$

where each matrix element in the Hamiltonian $H_{3\times3}$ can be written as a second-order polynomial in k_z:

$$H_{3\times3}=H^{(2)}k_z^2+H^{(1)}(k_\rho)k_z+H^{(0)}(k_\rho), \tag{15}$$

where the $H^{(n)}$ are 3×3 matrices whose elements are polynomial at most quadratic in (k_x,k_y,k_z). The explicit forms of the matrices $H^{(2)}$, $H^{(1)}$, and $H^{(0)}$ are given in Appendix A.

To solve the eigenvalue problem associated with Hamiltonian (15), we first transform it into a standard eigenvalue problem for k_z.[13,14] The energy-dispersion relations for holes in the heavy-hole light-hole, and SO bands can then be obtained by solving the eigenvalue problem

$$\begin{bmatrix} 0 & 1 \\ -(H^{(2)})^{-1}(H^0(k_\rho)-E) & (H^{(2)})^{-1}H^{(1)}(k_\rho) \end{bmatrix}\begin{bmatrix} \mathbf{F}_k \\ k_z\mathbf{F}_\mathbf{k} \end{bmatrix} = k_z\begin{bmatrix} \mathbf{F}_\mathbf{k} \\ k_z\mathbf{F}_\mathbf{k} \end{bmatrix}. \tag{16}$$

This last equation has six eigenvalues and six corresponding eigenvectors. Three solutions correspond to solutions propagating from left to right. The other three solutions for k_z are just the negative of the first three solutions and correspond to hole propagation from right to left.

Next, we consider tunneling of a heavy hole between two contacts sandwiching an arbitrary heterostructure. The wave function for a heavy hole (HH) incident from the left can be written as

$$\psi_{\mathrm{HH}}(r)=\begin{bmatrix} F_{1H} \\ F_{2H} \\ F_{3H} \end{bmatrix}e^{i(\mathbf{k}_\rho\cdot\boldsymbol{\rho}+k_z^{(h)}z)}, \tag{17}$$

and the reflected wave can be written as

$$\psi_{\mathrm{refl}}(\mathbf{r})=\Gamma_{\mathrm{HH}}\begin{bmatrix} F_{1H}^- \\ F_{2H}^- \\ F_{3H}^- \end{bmatrix}e^{i(\mathbf{k}_\rho\cdot\boldsymbol{\rho}-k_z^{(h)}z)} + \Gamma_{LH}\begin{bmatrix} F_{1L}^- \\ F_{2L}^- \\ F_{3L}^- \end{bmatrix}e^{i(\mathbf{k}_\rho\cdot\boldsymbol{\rho}-k_z^{(1)}z)} + \Gamma_{\mathrm{SO}}\begin{bmatrix} F_{1\mathrm{SO}}^- \\ F_{2\mathrm{SO}}^- \\ F_{3\mathrm{SO}}^- \end{bmatrix}e^{i(\mathbf{k}_\rho\cdot\boldsymbol{\rho}-k_z^{(so)}z)}, \tag{18}$$

where $(\Gamma_{\mathrm{HH}},\Gamma_{\mathrm{LH}},\Gamma_{\mathrm{SO}})$ are the reflection amplitudes for the incident heavy hole to be reflected in the heavy-hole light-hole and SO bands, respectively. The $(F_{1i}^-,F_{2i}^-,F_{3i}^-)$ with $(i=\mathrm{HH,LH,SO})$ are the components of the wave vector solutions of Eq. (16) for holes propagating from right to left.

In the transmitted region in which the potential energy profile can be different from the left contact, the transmitted wave function can be written as

$$\psi_{\mathrm{trans}}(\mathbf{r})=\tau_{\mathrm{HH}}\begin{bmatrix} F_{1H}^t \\ F_{2H}^t \\ F_{3H}^t \end{bmatrix}e^{i(\mathbf{k}_\rho\cdot\boldsymbol{\rho}+k_{z;t}^{(h)}z)} + \tau_{\mathrm{LH}}\begin{bmatrix} F_{1L}^t \\ F_{2L}^t \\ F_{3L}^t \end{bmatrix}e^{i(\mathbf{k}_\rho\cdot\boldsymbol{\rho}+k_{z;t}^{(l)}z)} + \tau_{\mathrm{SO}}\begin{bmatrix} F_{1\mathrm{SO}}^t \\ F_{2\mathrm{SO}}^t \\ F_{3\mathrm{SO}}^t \end{bmatrix}e^{i(\mathbf{k}_\rho\cdot\boldsymbol{\rho}+k_{z;t}^{(so)}z)}, \tag{19}$$

where the label t is a reminder that the quantities must be evaluated in the transmitted region. In Eq. (19), τ_{HF}, τ_{LH}, and τ_{SO} are the transmission coefficients from the heavy hole into the heavy-hole, light-hole, and SO bands in the transmitted region, respectively.

An arbitrary valence-band energy profile can always be approximated as a series of small steps in which the valence-band edge is assumed to be a constant. At the interface between any two steps, the envelope-function components (F_1,F_2,F_3) must be chosen such that

$$\begin{bmatrix} F_1(z) \\ F_2(z) \\ F_3(z) \end{bmatrix} \tag{20}$$

and

$$\begin{bmatrix} 2(\gamma_1-2\gamma_2)k_z & -2i\sqrt{3}\gamma_3k_\rho & i\sqrt{6}\gamma_3k_\rho \\ 2i\sqrt{3}\gamma_3k_\rho & 2(\gamma_1+2\gamma_2)k_z & -4\sqrt{2}\gamma_2k_z+3i\sqrt{2}\gamma_3k_\rho \\ -i\sqrt{6}\gamma_3k_\rho & -4\sqrt{2}\gamma_2k_z-3i\sqrt{2}\gamma_3k_\rho & 2\gamma_1k_z \end{bmatrix}\begin{bmatrix} F_1(z) \\ F_2(z) \\ F_3(z) \end{bmatrix}. \tag{21}$$

are continuous.[15] In Eq. (21), $k_z=-i(d/dz)$ and k_ρ is the magnitude of the in-plane wave vector. Conditions (20) and (21) are required for the wave function and the current density to be continuous across the interface. Expressions for the current density operator components are given in the appendixes.[8,12]

In order to calculate the transmission and reflection coefficients of holes incident from the left contact, the probability current density must be calculated along the growth direction for the incident, reflected, and transmitted waves. The transmission coefficients for a heavy hole incident from the left are then calculated as follows:

$$T_{\rm HH}=\frac{|\tau_{\rm HH}|^2 j_{z,H}^{\rm trans}}{j_{z,H}^{\rm inc}},\quad T_{\rm LH}=\frac{|\tau_{LH}|^2 j_{z,L}^{\rm trans}}{j_{z,H}^{\rm inc}},$$

$$T_{\rm SOH}=\frac{|\tau_{\rm SO}|^2 j_{z,\rm SO}^{\rm trans}}{j_{z,H}^{\rm inc}}, \tag{22}$$

and the reflection coefficients are

$$R_{\rm HH}=-\frac{|\Gamma_{\rm HH}|^2 j_{-z,H}^{\rm inc}}{j_{z,H}^{\rm inc}},\quad R_{\rm LH}=-\frac{|\Gamma_{LH}|^2 j_{-z,L}^{\rm inc}}{j_{z,H}^{\rm inc}},$$

$$R_{\rm SOH}=-\frac{|\Gamma_{\rm SO}|^2 j_{-z,\rm SO}^{\rm inc}}{j_{z,H}^{\rm inc}}. \tag{23}$$

In Eqs. (22) and (23), the labels inc and trans mean that the probability current density must be evaluated in the incident and transmitted regions, respectively. Furthermore, the relationship $j_{-z,\alpha}=-j_{z,\alpha}$ holds between the probability current densities corresponding to left ($j_{-z,\alpha}$) and right ($j_{z,\alpha}$) propagating states ($\alpha=H,L$, or SO). Current conservation further requires that $T_{\rm HH}+T_{\rm LH}+T_{\rm SOH}+R_{\rm HH}+R_{\rm LH}+R_{\rm SOH}=1$, which is helpful to check the accuracy of the numerical simulations. The tunneling problem described above can then be easily repeated for holes incident from the left contact in the light-hole or SO band. Next, we apply the formalism described above to the analysis of the tunneling of holes through a one-dimensional δ-scatterer and through abrupt heterointerfaces (in the $Al_xGa_{1-x}As/GaAs$ and $InP/In_yGa_{1-y}As$ material systems).

III. RESULTS

E-$\mathbf{k}$ relationship: First we consider an $In_yGa_{1-y}As$ region latticed matched to InP. In this case, the indium mole fraction y is equal 0.53. In Fig. 1 we plot the real (Re k_z) and imaginary (Im k_z) parts of the heavy-hole, light-hole, and SO bands as a function of the incident energy for a given magnitude of the transverse wave vector. For comparison, we also show the real and imaginary parts of the hole bands obtained while neglecting the SO band. The latter curves were calculated starting with the 4×4 Luttinger-Kohn Hamiltonian. In the axial approximation, this Hamiltonian can also be block diagonalized in two 2×2 Hamiltonians (upper and lower Hamiltonians). In this casse, the upper Hamiltonian is formed of the four upper left matrix elements in Hamiltonian (8).[2,10]

In Fig. 1, the zero of energy is the top of the valence band. The critical energies (E_h^-,E_h^+,E_1,$E_{\rm SO}$) are the values at which there is a sudden break in the energy dependence of the real and imaginary parts of the heavy-, light-, and SO-hole wave vectors. More precisely, E_h^- is the lowest positive energy at which $k_z^{(h)}$ is purely real; E_h^+ is the lowest positive energy at which Im $k_z^{(l)}$ becomes equal to zero, E_1 is the energy above which $k_z^{(l)}$ is purely real, and $E_{\rm SO}$ is the energy above which $k_z^{(\rm SO)}$ is purely real. Analytical expressions for (E_h^-,E_h^+,E_1) were derived in Ref. 2 when the SO band is neglected.[16]

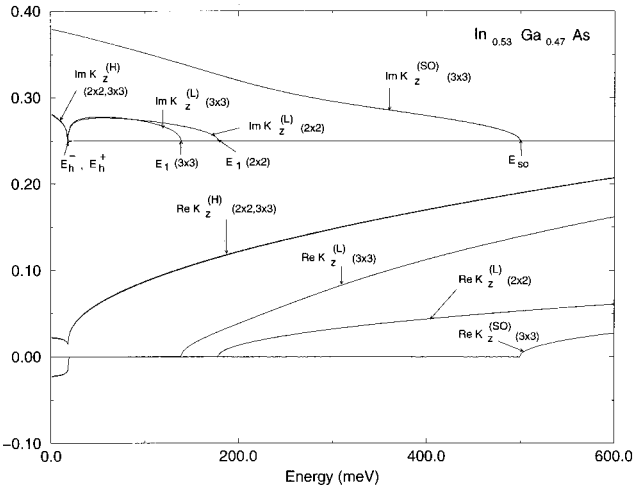

FIG. 1. Real and imaginary parts of the hole wave vectors solutions of the eigenvalue problem in Eq. (16) for a bulk $In_{0.53}Ga_{0.47}As$ region as a function of energy for a value of $k_\rho=0.04\ (2\pi/a)$ (a is 5.83 Å, the lattice constant of InP). The zero of energy is the top of the valence band. The real and imaginary parts are expressed in units of $2\pi/a$. For clarity, the imaginary parts have been shifted vertically by an amount equal to 0.25 $(2\pi/a)$. Also shown are the results obtained while neglecting the effects of spin-orbit coupling (Refs. 2 and 10) (curves labeled with the 2×2 symbol). The energies (E_h^-,E_h^+,E_1,$E_{\rm SO}$) defined in the text are also shown.

The following features are readily seen in Fig. 1: when $\mathbf{k}_\rho$ is nonzero, the heavy-hole dispersion relation is basically unchanged with the inclusion of the SO band, but the light-hole dispersion relation is strongly affected. Figure 1 shows that the energy threshold for purely propagating states for light holes occurs at a lower energy compared to the case when the SO band is neglected. A similar feature has been reported by Chao and Chuang in their study of SO interaction of the valence-band structure of strained semiconductor quantum wells.[4] The change in the energy threshold for propagating light holes affects the reflection coefficient for a light hole, but also the energy dependence of the amount of heavy- to light-hole conversion, as will be shown below. Furthermore, since the matrix elements (1,3) and (2,3) in Hamiltonian (8) are nonzero when $\mathbf{k}_\rho$ is nonzero, we expect some conversion from a heavy-hole (and light-hole) band to a SO band past the energy threshold for free propagating states in the SO band. This will be illustrated in the numerical examples below.

The energies (E_h^-,E_h^+,E_1,$E_{\rm SO}$) are functions of the magnitude of the transverse wave vector $\mathbf{k}_\rho$. These variations with k_ρ were determined numerically and are plotted in Fig. 2. In this figure, we also compare the k_ρ dependence of

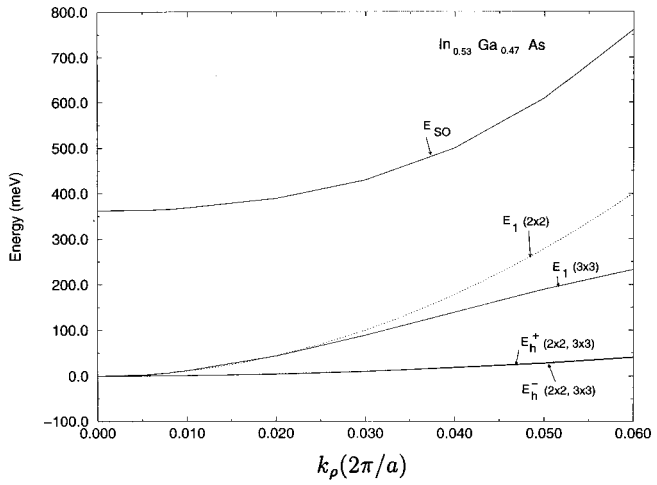

FIG. 2. Dependence on the magnitude of the transverse wave vector (k_ρ) of the energies ($E_h^-, E_h^+, E_1, E_{SO}$). Also shown as dashed lines are the k_ρ dependence of (E_h^-, E_h^+, E_1) when the effects of spin-orbit coupling are neglected (Refs. 2 and 10).

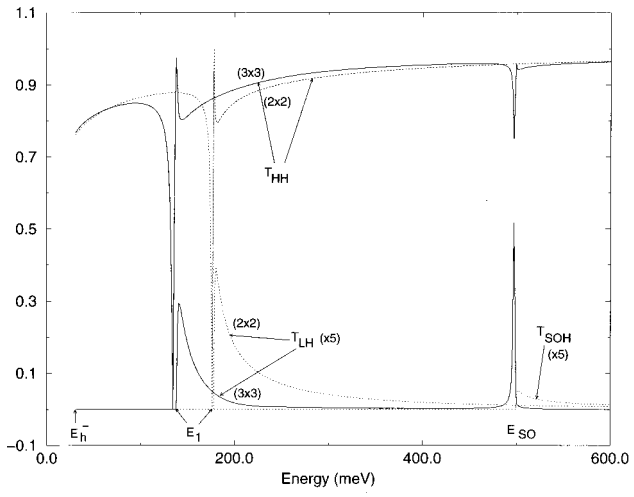

FIG. 3. Transmission coefficients of a heavy hole through a one-dimensional δ scatterer of strength $\Gamma\delta(z)$ with $\Gamma=-1$ eV Å. The in-plane wave vector is set equal to $k_\rho=0.04\,(2\pi/a)$ (where a is 5.83 Å, the lattice constant of InP). For clarity, the transmission coefficients T_{LH} and T_{SOH} for the heavy hole to be transmitted in the light-hole and SO bands, respectively, have been multiplied by a factor 5. Also shown as dashed lines are the transmission amplitudes calculated while neglecting the effects of the SO band.

(E_h^-, E_h^+, E_1) with the analytical results obtained while neglecting the effects of the SO band.[2]

Example 1: Tunneling through a δ scatterer. We consider tunneling of holes through a one-dimensional δ scatterer. This amounts to adding the potential-energy term $V_h(z)=\Gamma\delta(z)$ to the diagonal elements Hamiltonian (8), where Γ is the strength of the one-dimensional δ scatterer. If Γ is selected as negative, this potential energy approximately models the potential energy due to a uniform sheet of acceptors in a plane perpendicular to the direction of growth of an heterostructure in the assumption of strong screening, i.e., for heavily doped samples.

Integrating both sides of Eq. (14) from $z=0_-$ to $z=0_+$, we obtain the following set of equations relating the components of the envelope wave function on either sides of the δ scatterer:

$$(\Gamma_1-2\Gamma_2)[F_1'(0_+)-F_1'(0_-)]-\Gamma F_1(0_+)=0, \quad (24)$$

$$(\Gamma_1+2\Gamma_2)[F_2'(0_+)-F_2'(0_-)] - 2\sqrt{2}\Gamma_2[F_3'(0_+)-F_3'(0_-)]-\Gamma F_2(0_+)=0, \quad (25)$$

$$\Gamma_1[F_3'(0_+)-F_3'(0_-)] - 2\sqrt{2}\Gamma_2[F_2'(0_+)-F_2'(0_-)]-\Gamma F_3(0_+)=0. \quad (26)$$

Using the scattering states in Eqs. (17)–(19), the continuity of the components of the wave function and the three equations above lead to a matrix equation which must be solved for the unknown reflection ($\Gamma_{HH}, \Gamma_{LH}, \Gamma_{SOH}$) and transmission amplitudes ($\tau_{HH}, \tau_{LH}, \tau_{SOH}$):

$$M[\Gamma_{HH}, \Gamma_{LH}, \Gamma_{SOH}, \tau_{HH}, \tau_{LH}, \tau_{SOH}]^T=\mathbf{V}_h, \quad (27)$$

where T stands for the transpose operation. The explicit forms of M and $\mathbf{V}_h$ are given in Appendix B. The analysis can be easily repeated for holes incident either in the light-hole or SO band.

As an example, we consider tunneling through a δ scatterer with a strength of $\Gamma=-1$ eV Å in a region of bulk $In_{0.53}Ga_{0.47}As$. Figure 3 is a plot of the tunneling coefficients as a function of energy for an incident heavy hole with an in-plane wave vector equal to $4\times10^{-2}(2\pi/a)$. Also shown as dashed lines are the transmission coefficients calculated while neglecting the SO band.

Figure 3 indicates the presence of antiresonance/resonance pairs in the energy dependence of the transmission coefficient T_{HH}. The first antiresonance/resonance pair is observed in the energy range (E_h^-, E_1) where only the heavy holes are freely propagating on either side of the δ scatterer. Within this energy range, both the light-hole and SO states are quasiconfined, as shown in Fig. 1. This phenomenon is usually referred to as a Fano resonance in which a resonance/antiresonance pair occurs in the transmission through a scattering potential when a discrete (bound) state is coupled to a continuum.[17–19] The first antiresonance/resonance pair appears at a lower energy when the SO band is included in agreement with the shift toward lower energy of the energy threshold for light-hole propagation. A similar antiresonance/resonance structure was recently reported in the transmission coefficient T_{HH} of holes across a finite potential well.[9]

A second antiresonance/resonance pair appears just below E_{SO}. In that case, T_{HH} does not reach 0 and 1 at the antiresonant and resonant energies, respectively. This is probably related to the fact that the freely propagating hole is coupled to a freely propagating light hole and to an evanescent SO state just below E_{SO}. Because of the mismatch between the wave vectors of the two propagating states, the conditions are probably not quite right to observe a perfect antiresonance. This point would need to be investigated further.

Another interesting feature in Fig. 3 is the fact that T_{HH}

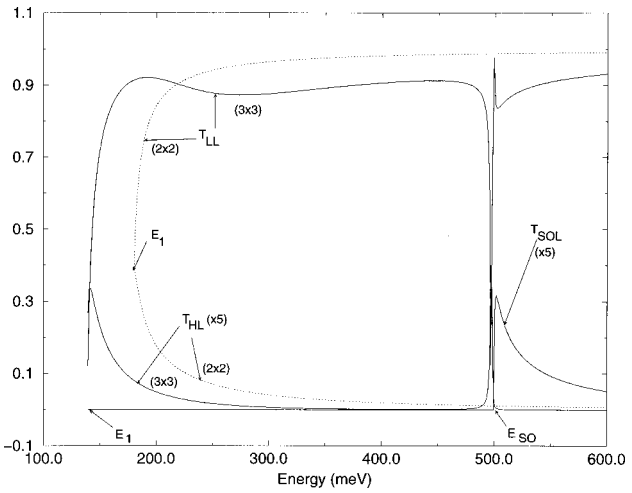

FIG. 4. Same as Fig. 3 for a light hole incident on a one-dimensional δ scatterer of strength $\Gamma\delta(z)$ with $\Gamma=-1$ eV Å. The in-plane wave vector is set equal to $k_\rho=0.04\ (2\pi/a)$ (where a is 5.83 Å, the lattice constant of InP). For clarity, the transmission amplitudes T_{HL} and T_{SOL} for the light hole to be transmitted in the heavy-hole and SO bands, respectively, have been multiplied by a factor 5. Also shown as dashed lines are the transmission amplitudes calculated while neglecting the effects of the SO band.

does not go down to zero at E_h^-, the threshold energy for a freely propagating heavy hole. Referring to Fig. 1, this is due to the fact that Re $k_z^{(h)}$ is nonzero at this energy despite the fact that Im $k_z^{(h)}$ is exactly zero beyond the point. The transmission coefficient T_{HH} only reaches zero at E_h^- when $k_\rho=0$, and there is no more coupling between the different hole bands.

Referring to Fig. 3, the probabilities for heavy-hole-to light-hole-or heavy-hole-to SO-band conversion are quite small. These probabilities were multiplied by a factor 5 in Fig. 3 to be easily seen. Figure 3 shows that T_{LH} reaches a maximum of 0.1 at the energy of the second antiresonance just below E_{SO}, despite the fact that the probabilities for hole conversion are quite small, We stress the fact that coupling between the hole bands is responsible for the observation of the antiresonance/resonance pairs, a feature not present in the tunneling of electrons through one-dimensional δ scatterers.

Figure 4 shows the transmission coefficients for holes incident in the light-hole band. The results are shown for energy above the threshold energy for free propagation ($E>E_1$) of light holes. The T_{LL} curve shifts towards lower energy when the effects of the SO band are included, as observed in Fig. 3 for heavy holes. In addition, the transmission coefficient T_{LL} is lower when the effects of SO band are included, whereas T_{HH} is more or less the same far from the antiresonance/resonance pairs. This is due to the much stronger coupling between light-hole and SO bands, as illustrated in Fig. 1. There is only one antiresonance/resonance pair in the energy dependence of T_{LL} located slightly below E_{SO}. This antiresonance/resonance pair has sharper features than the second antiresonance/resonance pair for the incident heavy holes observed in Fig. 3, because the incident light hole is more strongly coupled to the evanescent SO state just below E_{SO}. Finally, the transmission coefficients T_{HL} and T_{SOL} are also found to be quite small.

TABLE I. Luttinger-Kohn parameters and spin-orbit split-off energy used in the simulations. The corresponding values for $Al_xGa_{1-x}As$ and $In_yGa_{1-y}As$ materials are found by linear interpolation.

	GaAs	AlAs	InAs	InP
γ_1	6.85	3.45	20.4	4.95
γ_2	2.1	0.68	8.3	1.65
γ_3	2.9	1.29	9.1	2.35
Δ (eV)	0.34	0.28	0.38	0.1

Example 2: Tunneling through a potential step. Next, we consider the problem of hole tunneling across a potential step. Such a valence-band profile roughly approximates the valence band across the emitter-base junction of a *Pnp* heterojunction bipolar transistor (HBT) under high enough forward bias.[10] We consider two potential steps corresponding to the two lattice-matched interfaces $Al_{0.3}Ga_{0.7}As/GaAs$ and $InP/In_{0.53}Ga_{0.47}As$, which are two of the most widely used structures for HBT technology. For these materials, the values of the Luttinger-Kohn parameters and split-off energy are listed in Table I. The parameters for the ternary compound $In_yGa_{1-y}As$ and $Al_xGa_{1-x}As$ are obtained by linear interpolation from the parameters for the binaries.[20–22]

An important difference exists between the two heterojunctions as shown in Fig. 5. For the $Al_{0.3}Ga_{0.7}As/GaAs$ system, the valence-band discontinuity is much smaller than the spin-orbit split-off energy. Holes incident from the left need a kinetic energy of around 200 meV before being able to reach the threshold energy for free propagation in the SO band in the transmitted region. On the other hand, tunneling through the $InP/In_{0.53}Ga_{0.47}As$ will be very sensitive to presence of the SO band because the spin-orbit split-off energy in the transmitted region ($In_{0.53}Ga_{0.47}As$) is smaller than the

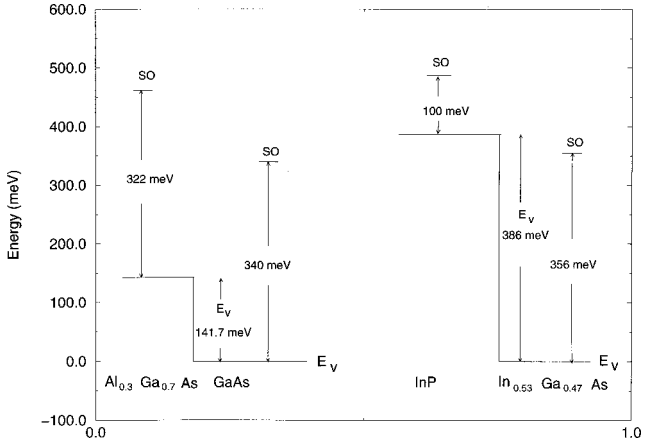

FIG. 5. Illustration of the valence-band discontinuity across the $Al_{0.3}Ga_{0.7}As/GaAs$ and $InP/In_{0.53}Ga_{0.47}As$ interfaces. The horizontal lines labeled ''SO'' are the locations of the spin-orbit split-off energy-band minimum on both sides of the structure. The energy threshold E_{SO} for free propagation in the SO band coincides with the SO level for $k_\rho=0$, but shifts upward in energy as the magnitude of the transverse wave vector increases, as shown in Fig. 1.

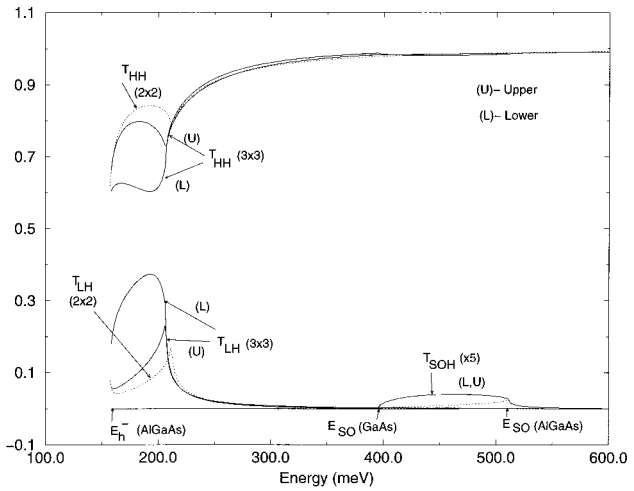

FIG. 6. Transmission coefficients of a heavy hole incident from the left side of the $Al_{0.3}Ga_{0.7}As/GaAs$ potential step shown in Fig. 5. The results are shown for the upper and lower 3×3 Hamiltonian. The valence-band discontinuity is set equal to $\Delta E_v = 141.7$ meV. The in-plane wave vector is set equal to $k_\rho = 0.04\ (2\pi/a)$ (where a is 5.6566 Å, the lattice constant of GaAs). Also shown are the results obtained with the upper and lower Hamiltonians when the effects of the SO band are included. For clarity, the results are not shown for the lower 2×2 Hamiltonian.

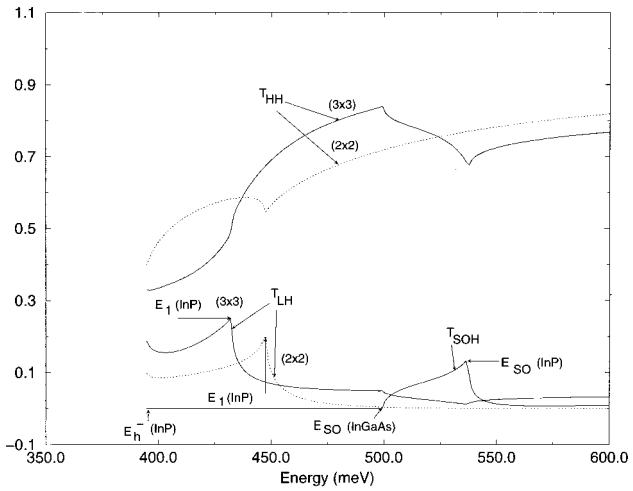

FIG. 7. Transmission coefficients for a heavy hole incident on the $InP/In_{0.53}Ga_{0.47}As$ interface shown in Fig. 5. Also shown are the transmission coefficients calculated while neglecting the effects of the SO band. The results are shown for the upper Hamiltonians only. The valence-band discontinuity is set equal to $\Delta E_v = 346$ meV. The materials parameters are listed in Table I. The in-plane wave vector is set equal to $k_\rho = 0.04\ (2\pi/a)$ (where a is 5.83 Å, the lattice constant of InP).

valence-band discontinuity ($\Delta E_v = 386$ meV). Furthermore, the spin-orbit split-off energy in the left region (InP) is quite small (100 meV) and the dispersion relation for heavy and light holes in this region will be strongly affected by the SO band even for holes with low incident kinetic energy.

Applying boundary conditions (20) and (21) and using the wave functions (17)–(19) on the left and right sides of the step, respectively, the unknown reflection and transmission amplitudes Γ_{HH}, Γ_{LH}, Γ_{SO}, τ_{HH}, τ_{LH}, and τ_{SO} can be found as solutions of a matrix equation of the form given in Eq. (27). Since the potential steps in Fig. 5 lacks inversion symmetry, the transmission coefficients will be different when calculated with the upper or lower Hamiltonians. This will be illustrated in the numerical examples below.

Hereafter, we only consider the transmission coefficients of heavy holes incident from left to right on the potential steps shown in Fig. 5. In a Pnp HBT, heavy holes would constitute the major component of the injected current across a forward biased emitter (*P*-type)/base (*n*-type) junction.

Case 1: The $Al_{0.3}Ga_{0.7}As/GaAs$ *interface.* Figure 6 shows the transmission coefficients as a function of energy for holes incident from left to right on the structure shown on the left in Fig. 5. The lines labeled (*U*) and (*L*) are the results obtained with the upper and lower 3×3 Hamiltonians, respectively. Also shown are the results obtained with the upper Hamiltonian when the SO band is neglected. Figure 6 indicates that both T_{HH} and T_{LH} are not very much affected by the inclusion of the SO band at energy above the threshold energy E_1 for free propagation in the light-hole band in the $Al_xGa_{1-x}As$ region. Below E_1, there is a substantial difference between the results for T_{HH} and T_{LH} obtained with the lower and upper Hamiltonians. This is expected since a potential step lacks inversion symmetry, and results from the upper and lower Hamiltonians are not expected to be identical in that case.[2] The lower the kinetic energy of the incident hole, the more drastic the importance of the valence-band discontinuity and the larger is the discrepancy in the results with the upper and lower Hamiltonians. For energy above E_1, the results with the upper and lower Hamiltonians are in close agreement.

Furthermore, Fig. 6 shows that the probability of heavy- to SO-band (T_{SOH}) transition across the interface is fairly small. This feature results from the fact that the threshold energy for free propagation in the SO band is quite high. It is about 500 meV for the incident heavy hole with an in-plane wave vector $k_\rho = 4\times10^{-2}2\pi/a$ considered here. As a result, we do not expect a large difference between the transmission coefficients calculated with and without the effects of the SO band.

Case 2: The $InP/In_{0.53}Ga_{0.47}As$ *interface.* The situation is quite different for the second interface shown in Fig. 5. As shown in Fig. 7, the energy dependence of the transmission coefficients for an incident heavy hole is markedly different whether or not the effects of the SO band are included. The results in Fig. 7 are for the upper (2×2 and 3×3) Hamiltonians only. Figure 8 shows that for that interface the results obtained with the upper and lower (3×3) Hamiltonians are quite different over the full range of incident energy investigated here.

In Figs. 7 and 8, there are cusps in the transmission coefficient T_{HH} appearing at an incident energy equal to the threshold energies for free propagation in the SO bands on either side of the interface. T_{SOH} is nonzero past the energy threshold E_{SO} in the $In_yGa_{1-y}As$ region (around 500 meV according to Fig. 1). However, T_{SOH} goes back down close to zero above 535 meV because there is a finite probability to be reflected in the SO band in the InP region beyond that energy.

Figures 9 and 10 are plots similar to Figs. 7 and 8 for a light hole incident from the InP region. Figure 9 shows that

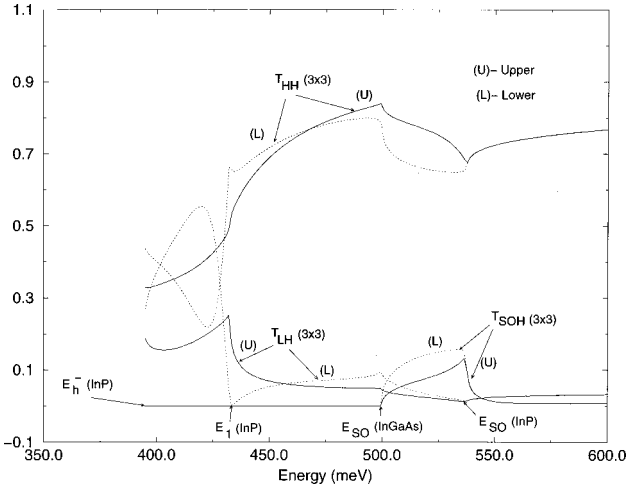

FIG. 8. Transmission coefficients for a heavy hole incident on the InP/$In_{0.53}Ga_{0.47}As$ interface shown in Fig. 5. Comparison of the transmission coefficients obtained with the upper and lower 3×3 Hamiltonians. All parameters are the same as in the caption of Fig. 7.

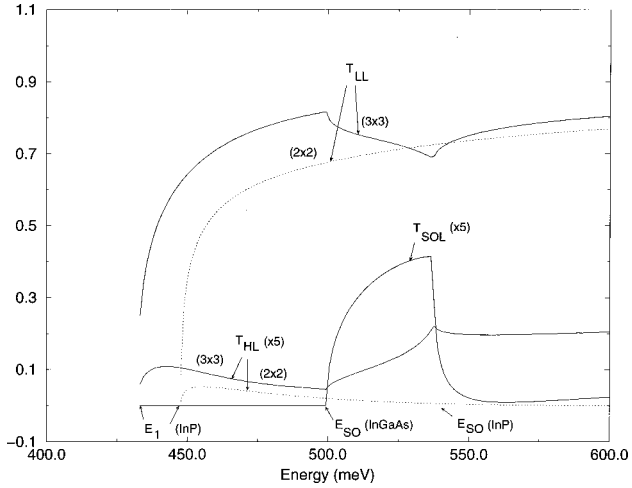

FIG. 9. Same as Fig. 6 for a light hole incident on the InP/$In_{0.53}Ga_{0.47}As$ potential step shown in Fig. 5. All parameters are the same as in the caption of Fig. 6. Also shown are the transmission and reflection coefficients calculated while neglecting the effects of the SO band.

the probability of light- to heavy-hole conversion is much smaller than the probability of heavy- to light-hole conversion shown in Fig. 5. This is expected using a simple estimate based on the well-known result for electron tunneling through a potential step

$$T_{ji}=\frac{2k_j^{\mathrm{trans}}/k_i^{\mathrm{inc}}}{[k_j^{\mathrm{trans}}/k_i^{\mathrm{inc}}+1]^2}, \tag{28}$$

where $ji=$HL or LH for an incident light and heavy hole, respectively. In Eq. (28), the ratio of the of the z-component of the wave vectors is smaller when $ij=$HL, which explains why T_{HL} is smaller than T_{LH}.

IV. CONCLUSIONS

We have used the 6×6 Luttinger-Kohn Hamiltonian to study the effects of the spin-orbit split-off band on the transmission and reflection coefficients of holes through various heterostructures. The tunneling and reflection coefficients of heavy and light holes were calculated using the upper and lower Hamiltonians obtained through a unitary transform of the 6×6 Luttinger-Kohn Hamiltonian.

We have shown that SO interaction has a more profound influence on the light-hole energy dispersion relation than on the heavy-hole energy dispersion relation. More specifically, the energy threshold (E_1) for free propagating light-hole states was found to occur at a lower energy compared to the value obtained when the effects of SO interaction are neglected. We have studied the tunneling of holes through one-dimensional δ scatterers and potential steps. These examples show that the effects of SO interaction can influence the tunneling of heavy-holes even at energies far below the threshold energy for free propagation in the SO band. This is due to the lowering of the threshold energy for free propagation in the light-hole band resulting from a strong coupling between the light-hole and SO bands for holes incident on a heterointerface with a nonzero in-plane wave vector.

For the case of tunneling through a one-dimensional δ scatterer, we have found the presence of antiresonance/resonance pairs (Fano resonances) in the energy dependence of the heavy- and light-hole transmission coefficients. These antiresonance/resonance pairs occur slightly below the threshold energies (E_1 and E_{SO}) for heavy holes, and slightly below E_{SO} for light holes.

For the case of potential steps, the effects of the SO band on hole tunneling coefficients were found to be minor in the case of an $Al_{0.3}Ga_{0.7}As$/GaAs interface but quite drastic in the case of an InP/$In_{0.53}Ga_{0.47}As$ potential step. This is due to the much lower values of the threshold energy for free propagation in the SO band on either side of the heterointerface in the InP/$In_{0.53}Ga_{0.47}As$ system, as illustrated in Fig. 8. Our results indicate that the SO band cannot be neglected in the calculation of the emitter injection efficiency of Pnp HBTs using InP/$In_{0.53}Ga_{0.47}As$ materials for the emitter-base junction. In that case, the valence-band energy profile through the emitter-base junction under large enough emitter-base bias

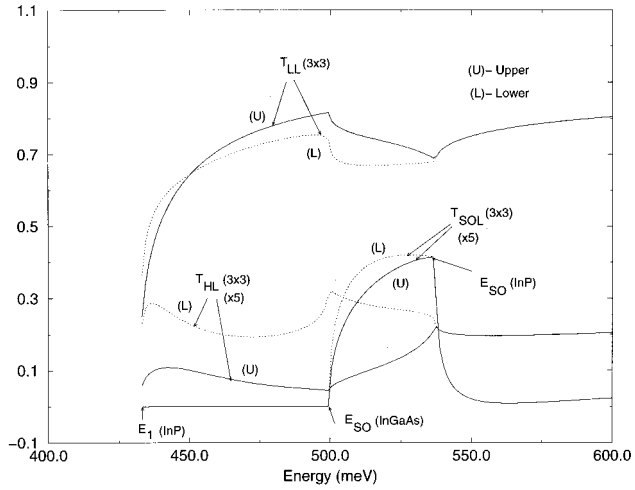

FIG. 10. Same as Fig. 8 for a light hole incident on the InP/$In_{0.53}Ga_{0.47}As$ potential step shown in Fig. 5. All parameters are the same as in the caption of Fig. 6.

approaches the step potential analyzed here.[10] Because of the probability of hole conversion at the interface (especially heavy to light) the effects of the SO band also affects the energy distribution of the heavy-holes injected in the base of the Pnp HBTs. The latter controls the HBT base transit time which is one of the leading components affecting the high-frequency performance of these devices.[23]

ACKNOWLEDGMENTS

This work was supported by the National Science Foundation (Grant No. ECS-9525942). We also acknowledge the Ohio-Cray supercomputing center for the use of their facilities.

APPENDIX A: EIGENVALUES AND EIGENVECTORS OF THE $H_{3\times3}$ HAMILTONIAN

The 6×6 Luttinger-Kohn Hamiltonian (1) can be block diagonalized using a unitary transformation[2]

$$H=\begin{bmatrix} H_{3\times3} & 0 \\ 0 & H_{3\times3}^{\dagger} \end{bmatrix}, \tag{A1}$$

where $H_{3\times3}^{\dagger}$ is the Hermitian conjugate of $H_{3\times3}$.

$$H_{3\times3}=\begin{bmatrix} P+Q & -R_\rho-iS_\rho & -\sqrt{2}R_\rho+\dfrac{i}{\sqrt{2}}S_\rho \\ -R_\rho+iS_\rho & P-Q & \sqrt{2}Q+\dfrac{i}{\sqrt{3/2}}S_\rho \\ -\sqrt{2}R_\rho-\dfrac{i}{\sqrt{2}}S_\rho & \sqrt{2}Q-\dfrac{i}{\sqrt{3/2}}S_\rho & P+\Delta \end{bmatrix} \tag{A2}$$

This Hamiltonian can be rewritten as

$$H_{3\times3}=H^{(2)}k_z^2+H^{(1)}(k_\rho)k_z+H^{(0)}(k_\rho), \tag{A3}$$

where

$$H^{(2)}=\left(\frac{\hbar^2}{2m_0}\right)\begin{bmatrix} (\gamma_1-2\gamma_2) & 0 & 0 \\ 0 & (\gamma_1+2\gamma_2) & 0 \\ 0 & 0 & \gamma_1 \end{bmatrix}, \tag{A4}$$

$$H^{(1)}(k_\rho)=\left(\frac{\hbar^2}{2m_0}\right)\begin{bmatrix} 0 & -2i\sqrt{3}\gamma_3k_\rho & i\sqrt{6}\gamma_3k_\rho \\ 2i\sqrt{3}\gamma_3k_\rho & 0 & 3i\sqrt{2}\gamma_3k_\rho \\ -i\sqrt{6}\gamma_3k_\rho & -3i\sqrt{2}\gamma_3k_\rho & 0 \end{bmatrix}, \tag{A5}$$

and

$$H^{(0)}(k_\rho)=\left(\frac{\hbar^2}{2m_0}\right)\begin{bmatrix} (\gamma_1+\gamma_2)k_\rho^2 & \sqrt{3}\tilde{\gamma}k_\rho^2 & \sqrt{6}\tilde{\gamma}k_\rho^2 \\ \sqrt{3}\tilde{\gamma}k_\rho^2 & (\gamma_1-\gamma_2)k_\rho^2 & \sqrt{2}\gamma_2k_\rho^2 \\ \sqrt{6}\tilde{\gamma}k_\rho^2 & \sqrt{2}\gamma_2k_\rho^2 & \gamma_1k_\rho^2+\Delta \end{bmatrix}, \tag{A6}$$

where $\tilde{\gamma}=(\gamma_2+\gamma_3)/2$. The eigenvalue problem associated with the Hamiltonian $H_{3\times3}$ is more easily solved when recast in the eigenvalue problem for the wave vector k_z as described in the text [Eq. (16)].

With the decomposition of the Hamiltonian described above, the current density operator in the z direction can then be written as follows:[8]

$$J_z=\frac{1}{\hbar}\left(2H^{(2)}\frac{\delta}{\delta z}+H^{(1)}(k_\rho)\right). \tag{A7}$$

J_z is equal to Eq. (21) in the text multiplied by $\hbar^2/2m_0$. This expression is needed to calculate the reflection and transmission coefficients as outlined in Sec. II.

APPENDIX B: TUNNELING THROUGH A δ SCATTERER

Starting with Eqs. (24)–(26) and using Eqs. (17)–(19) describing the incident, reflected, and transmitted wave functions on either sides of the δ scatterer, the application of the boundary conditions (20) and (21) leads to the matrix equation

$$M[\Gamma_{\rm HH},\Gamma_{\rm LH},\Gamma_{\rm SO},\tau_{\rm HH},\tau_{\rm LH},\tau_{\rm SO}]^T=\mathbf{V}_h, \tag{B1}$$

where M is given by

$$M=\begin{bmatrix} F_{1h}^{-} & F_{1l}^{-} & F_{1\mathrm{so}}^{-} & -F_{1h} & -F_{1l} & -F_{1\mathrm{so}} \\ F_{2h}^{-} & F_{2l}^{-} & F_{2\mathrm{so}}^{-} & -F_{2h} & -F_{2l} & -F_{2\mathrm{so}} \\ F_{3h}^{-} & F_{3l}^{-} & F_{3\mathrm{so}}^{-} & -F_{3h} & -F_{3l} & -F_{3\mathrm{so}} \\ ik_z^{(h)}\Gamma^{-}F_{1h}^{-} & ik_z^{(l)}\Gamma^{-}F_{1l}^{-} & ik_z^{(\mathrm{so})}\Gamma^{-}F_{\mathrm{so}}^{-} & \delta^{(h)}F_{1h} & \delta^{(h)}F_{1l} & \delta^{(h)}F_{1\mathrm{so}} \\ ik_z^{(h)}\Gamma^{+}F_{2h}^{-} & ik_z^{(l)}\Gamma^{+}F_{2l}^{-} & ik_z^{(\mathrm{so})}\Gamma^{+}F_{2\mathrm{so}}^{-} & ik_z^{(h)}\Gamma+F_{2h}^{-} & ik_z^{(l)}\Gamma^{+}F_{2l}^{-} & ik_z^{(\mathrm{so})}\Gamma^{+}F_{2\mathrm{so}}^{-} \\ -2i\sqrt{2}\Gamma_2 k_z^{(h)}F_{3h}^{-} & -2i\sqrt{2}\Gamma_2 k_z^{(l)}F_{3l}^{-} & -2i\sqrt{2}\Gamma_2 k_z^{(\mathrm{so})}F_{3\mathrm{so}}^{-} & -2i\sqrt{2}\Gamma_2 k_z^{(h)}F_{3h}^{-} & -2i\sqrt{2}\Gamma_2 k_z^{(l)}F_{3l}^{-} & -2i\sqrt{2}\Gamma_2 k_z^{(\mathrm{so})}F_{3\mathrm{so}}^{-} \\ ik_z^{(h)}\Gamma^{+}F_{3h}^{-} & ik_z^{(l)}\Gamma^{+}F_{3l}^{-} & ik_z^{(\mathrm{so})}\Gamma^{+}F_{3\mathrm{so}}^{-} & ik_z^{(h)}\Gamma^{+}F_{3h}^{-} & ik_z^{(l)}\Gamma^{+}F_{3l}^{-} & ik_z^{(\mathrm{so})}\Gamma^{+}F_{3\mathrm{so}}^{-} \\ -2i\sqrt{2}\Gamma_2 k_z^{(h)}F_{2h}^{-} & -2i\sqrt{2}\Gamma_2 k_z^{(l)}F_{2l}^{-} & -2i\sqrt{2}\Gamma_2 k_z^{(\mathrm{so})}F_{2\mathrm{so}}^{-} & -2i\sqrt{2}\Gamma_2 k_z^{(h)}F_{2h}^{-} & -2i\sqrt{2}\Gamma_2 k_z^{(l)}F_{2l}^{-} & -2i\sqrt{2}\Gamma_2 k_z^{(\mathrm{so})}F_{2\mathrm{so}}^{-} \end{bmatrix}, \tag{B2}$$

where $\Gamma^{-}=\Gamma_1-2\Gamma_2$, $\Gamma^{+}=\Gamma_1+2\Gamma_2$, and the following notations were introduced:

$$\delta^{(h)}=ik_z^{(h)}\Gamma^{-}F_{1h}-\Gamma, \tag{B3}$$

$$\delta^{(l)}=ik_z^{(l)}\Gamma^{-}F_{1l}-\Gamma, \tag{B4}$$

$$\delta^{(\mathrm{so})}=ik_z^{(\mathrm{so})}\Gamma^{-}F_{1\mathrm{so}}-\Gamma, \tag{B5}$$

and $\mathbf{V}_h$ is given by

$$\begin{bmatrix} -F_{1h} \\ -F_{2h} \\ -F_{3h} \\ ik_z^{(h)}F_{1h}(\Gamma_1-2\Gamma_2) \\ ik_z^{(h)}F_{2h}(\Gamma_1-2\Gamma_2)-2i\sqrt{2}\Gamma_2 k_z^{(h)}F_{3h} \\ ik_z^{(h)}F_{3h}(\Gamma_1-2\Gamma_2)-2i\sqrt{2}\Gamma_2 k_z^{(h)}F_{2h} \end{bmatrix}. \tag{B6}$$

The matrix M is unchanged for an incident hole in the light-hole or SO band, but the vector $\mathbf{V}$ must be modified accordingly.

APPENDIX C: TUNNELING THROUGH A POTENTIAL STEP

Starting with Eqs. (17)–(19) describing the incident, reflected, and transmitted wave functions on either side of a potential step, the application of the boundary conditions (20) and (21) leads to the matrix equation

$$M[\Gamma_{\mathrm{HH}},\Gamma_{\mathrm{LH}},\Gamma_{\mathrm{SO}},\tau_{\mathrm{HH}},\tau_{\mathrm{LH}},\tau_{\mathrm{SO}}]^{T}=\mathbf{V}_h, \tag{C1}$$

where M is given by

$$M=\begin{bmatrix} F_{1h}^{-} & F_{1l}^{-} & F_{1\mathrm{so}}^{-} & -F_{1h}^{t} & -F_{1l}^{t} & -F_{1\mathrm{so}}^{t} \\ F_{2h}^{-} & F_{2l}^{-} & F_{2\mathrm{so}}^{-} & -F_{2h}^{t} & -F_{2l}^{t} & -F_{2\mathrm{so}}^{t} \\ F_{3h}^{-} & F_{3l}^{-} & F_{3\mathrm{so}}^{-} & -F_{3h}^{t} & -F_{3l}^{t} & -F_{3\mathrm{so}}^{t} \\ M_{41} & M_{42} & M_{43} & M_{44} & M_{45} & M_{46} \\ M_{51} & M_{52} & M_{53} & M_{54} & M_{55} & M_{56} \\ M_{61} & M_{62} & M_{63} & M_{64} & M_{65} & M_{66} \end{bmatrix}, \tag{C2}$$

where

$$M_{41}=i(\gamma_1-2\gamma_2)k_z^{(h)}F_{1h}^{-}-2\sqrt{3}\gamma_3 k_\rho F_{2h}^{-}+\sqrt{6}\gamma_3 k_\rho F_{3h}^{-}; \tag{C3}$$

M_{42} and M_{43} are obtained by changing the index h to l and so, respectively;

$$M_{44}=i(\gamma_1^{t}-2\gamma_2^{t})k_z^{(h)t}F_{1h}^{t}+2\sqrt{3}\gamma_3^{t}k_\rho F_{2h}^{t}-\sqrt{6}\gamma_3^{t}k_\rho F_{3h}^{t}; \tag{C4}$$

M_{45} and M_{46} are obtained by changing the index h to l and so, respectively;

$$M_{51}=2\sqrt{3}\gamma_3 k_\rho F_{1h}^{-}-i(\gamma_1+2\gamma_2)k_z^{(h)}F_{2h}^{-}+3\sqrt{2}\gamma_3 k_\rho F_{3h}^{-}-2i\sqrt{2}\gamma_2 k_z^{(h)}F_{3h}^{-}; \tag{C5}$$

M_{52} and M_{53} are obtained by changing the index h to l and so, respectively;

$$M_{54}=-2\sqrt{3}\gamma_3^{t}k_\rho F_{1h}^{t}+i(\gamma_1^{t}+2\gamma_2^{t})k_z^{(h)t}F_{2h}^{t}-3\sqrt{2}\gamma_3^{t}k_\rho F_{3h}^{t}-2i\sqrt{2}\gamma_2^{t}k_z^{(h)t}F_{3h}^{t}; \tag{C6}$$

M_{55} and M_{56} are obtained by changing the index h to l and so, respectively;

$$M_{61} = -\sqrt{6}\,\gamma_3 k_\rho F^-_{1h} - 3\sqrt{2}\,\gamma_3 k_\rho F^-_{2h} + i\,\gamma_1 k_z^{(h)} F^-_{3h} - 2i\sqrt{2}\,\gamma_2 k_z^{(h)} F^-_{2h}; \tag{C7}$$

$$M_{64} = \sqrt{6}\,\gamma_3^t k_\rho F^t_{1h} + 3\sqrt{2}\,\gamma_3^t k_\rho F^t_{2h} + i\,\gamma_1^t k_z^{(h)t} F^t_{3h} - 2i\sqrt{2}\,\gamma_2^t k_z^{(h)t} F^t_{2h}; \tag{C8}$$

M_{62} and M_{63} are obtained by changing the index h to l and so, respectively; and M_{65} and M_{66} are obtained by changing the index h to l and so, respectively. In Eq. (C1), $\mathbf{V}_h$ is given by

$$\begin{bmatrix} -F_{1h} \\ -F_{2h} \\ -F_{3h} \\ i(\gamma_1 - 2\gamma_2)k_z^{(h)} F_{1h} + 2\sqrt{3}\,\gamma_3 k_\rho F_{2h} - \sqrt{6}\,\gamma_3 k_\rho F_{3h} \\ -2\sqrt{3}\,\gamma_3 k_\rho F_{1h} + i(\gamma_1 + 2\gamma_2)k_z^{(h)} F_{2h} - 2i\sqrt{2}\,\gamma_2 k_z^{(h)} F_{3h} - 3\sqrt{2}\,\gamma_3 k_\rho F_{3h} \\ \sqrt{6}\,\gamma_3 k_\rho F_{1h} + 3\sqrt{2}\,\gamma_3 k_\rho F_{2h} - 2i\sqrt{2}\,\gamma_2 k_z^{(h)} F_{2h} + i\,\gamma_1 k_z^{(h)} F_{3h} \end{bmatrix}. \tag{C9}$$

For holes incident in the light-hole or SO band, only the vector $\mathbf{V}_h$ must be upgraded while solving Eq. (C1) by changing the index h to l or so, respectively.

[1] E. O. Kane, in *Physics of III-V Compounds*, edited by R. K. Willardson and A. C. Beer, Semiconductors and Semimetals, Vol. 1 (Academic, New York, 1966), p. 75.

[2] S. L. Chuang, Phys. Rev. B **40**, 10 379 (1989).

[3] R. Wessel and M. Altarelli, Phys. Rev. B **39**, 12 802 (1989).

[4] C. Y. Chao and S. L. Chuang, Phys. Rev. B **43**, 7027 (1991).

[5] The 6×6 Luttinger-Kohn Hamiltonian can be block diagonalized even when the axial approximation is not applied, as described, for instance, by E. P. O'Reilly, Semicond. Sci. Technol. **4**, 121 (1988).

[6] J. B. Xia, Phys. Rev. B **38**, 8365 (1988).

[7] J. Lee, C. Jagannath, M. O. Vassell, and E. S. Koteles, Phys. Rev. B **37**, 4164 (1988).

[8] Y. X. Liu, D. Z.-Y. Ting, and T. C. McGill, Phys. Rev. B **54**, 5675 (1996).

[9] A. D. Sanchez and C. R. Proetto, J. Phys.: Condens. Matter **7**, 2059 (1995).

[10] T. Kumar, M. Cahay, and K. Roenker, Phys. Rev. B **56**, 4836 (1997).

[11] C.-S. Chang and S. L. Chuang, IEEE J. Sel. Top. Quantum Electron. **1**, 218 (1995).

[12] A. D. Sanchez and C. R. Proetto, Phys. Rev. B **51**, 17 199 (1995).

[13] J. H. Wilkinson, *The Algebraic Eigenvalue Problem* (Oxford University Press, Oxford, 1965), pp. 633 and 634.

[14] Y. C. Chang and J. N. Schulman, Phys. Rev. B **25**, 3975 (1982).

[15] The boundary condition (21) was derived here following Ref. 8, starting with Eq. (23) in that paper.

[16] No attempt was made to derive the analytical dependence of $(E_h^-, E_h^+, E_1, E_{\mathrm{SO}})$ on k_ρ since it probably requires tedious expansions leading to intricate expressions. The latter were determined numerically, and the results are shown in Fig. 2.

[17] U. Fano, Phys. Rev. **124**, 1866 (1961).

[18] C. Kunze and P. F. Bagwell, Phys. Rev. B **51**, 13 410 (1995).

[19] T. B. Boykin, B. Pezeshki, and J. J. Harris, Phys. Rev. B **46**, 12 769 (1992).

[20] For the $Al_{0.3}Ga_{0.7}As/GaAs$ interface, we use $\Delta E_v = 0.4X(1.04x + 0.47x^2)$ with $x = 0.3$, following R. C. Miller, A. C. Gossard, D. A. Kleinman, and O. Munteanu, Phys. Rev. B **29**, 3740 (1984).

[21] C. D. Lee and S. R. Forrest, Appl. Phys. Lett. **57**, 469 (1990).

[22] For the $InP/In_{0.53}Ga_{0.47}As$ interface, we use 1.344 eV and $0.324 + 0.7x + 0.4x^2$ for the energy gaps of InP and $In_yGa_{1-y}As$, respectively. For the conduction- and valence-band offsets, we follow Ref. 21 and use $\Delta E_c = 0.36\ \Delta E_g$ and $\Delta E_v = 0.64\ \Delta E_g$.

[23] J. A. Hutchby, IEEE Electron Device Lett. **EDL-7**, 108 (1986).